Available online at www.sciencedirect.com
SCIENCE DIRECT®
Coordination Chemistry Reviews 238–239 (2003) 333–346
COORDINATION CHEMISTRY REVIEWS
www.elsevier.com/locate/ccr

Effects of the bridging ligands on the molecular and electronic structure of $Fe_2(CO)_9$ derivatives

Joachim Reinhold [a,*], André Barthel [a], Carlo Mealli [b]

[a] *Wilhelm-Ostwald-Institut für Physikalische und Theoretische Chemie, Universität Leipzig, D-04103 Leipzig, Germany*
[b] *Istituto per lo Studio della Stereochimica ed Energetica dei Composti di Coordinazione, C.N.R., I-50132 Firenze, Italy*

Received 4 March 2002; accepted 27 September 2002

Contents

Abstract

This article reviews the structural and electronic properties of $Fe_2(CO)_9$ derivatives with any triad of σ donor and π acceptor bridges selected from the series CO, CH_2, CF_2, $SiMe_2$, $GeMe_2$, InMe and CS. Based on the available structural data and computational results, the bridges other than CO can be catalogued in two different groups. The ligands of group I feature a pivotal carbon atom such as the CO ligand itself (i.e. L = CH_2, CF_2 and CS). Those of group II are characterized by different hetero-atoms at the core of the bridging group (i.e. L = $SiMe_2$, $GeMe_2$ and InMe). The geometry of the inner $Fe(\mu\text{-}L)_3Fe$ skeleton changes significantly between the members of the different series. In particular, the range of Fe–Fe distances can be as large as 52.3 pm, the higher and lower limits being found in the system with three InMe bridges and in that with one CO and two CF_2 ligands, respectively. It turns out that ligands of group I favor the decrease of the Fe–Fe distance compared to the parent compound $Fe_2(CO)_9$. On the contrary, those of group II favor a larger intermetallic separation. By detailed analyses, the structural effects can be traced back to the σ donor and π acceptor capabilities of the different bridges.

Keywords: Binuclear iron carbonyls; π Acceptor bridges; Metal–metal bonding, MO calculations

1. Introduction

Mono- and polynuclear carbonyl complexes are amongst the most investigated classes of compounds for their relevance in homogeneous catalysis and in the synthesis of new systems with unusual features [1]. In this respect, it is noteworthy that the CO ligands can be easily substituted for, especially at the bridging positions. For example, chemical species with potential σ donor and π acceptor capabilities (e.g. isonitriles, nitrogen monoxide and methylenes [2] as well as monovalent boron fragments BR (R = F, NH_2, NMe_2) [3]) may be found as alternative bridges between metal

* Corresponding author. Tel.: +49-341-973-6500; fax: +49-341-973-6399
E-mail address: reinhold@quant1.chemie.uni-leipzig.de (J. Reinhold).

0010-8545/02/$ - see front matter © 2002 Elsevier Science B.V. All rights reserved.
PII: S0010-8545(02)00282-5

centers. The methylene analogues SiR_2 [4] and GeR_2 (R = alkyl) [5] are known to occupy bridging positions. Also, iron species with bridging moieties based on the group III elements (e.g. RAl(I) (R = Cp*, alkyl) [6], RGa(I) (R = Cp*, alkyl, $C(SiMe_3)_3$) [7] and RIn(I) (R = $C(SiMe_3)_3$) [8]) have been synthesized. Finally, it has been recently found that CF_2 [9] is able to sit across the metals in binuclear iron compounds.

It appears that, in general, the carbonyl analogues prefer the bridging to the terminal position. Moreover, their substitution for CO exerts a very specific influence on the geometry of the bridged moiety. In particular, the metal–metal distances are typically affected. Only in part, this is attributable to the spatial demand of the new bridge. More often, the electronic properties of the ligand differ significantly from those of carbon monoxide and the consequences can be macroscopic.

In a recent paper, we have analyzed theoretically the stepwise substitution of bridging COs with alkylindium(I) groups in the series $(CO)_3Fe(\mu\text{-}CO)_{3-n}(\mu\text{-}InMe)_nFe(CO)_3$ ($n = 0, 1, 2, 3$) [10]. It has been found that the steady increase of the Fe–Fe distance, associated with the parallel decrease of the $Fe–CO_{terminal}$ distances, is due to both the different σ donor [$RIn(I) \gg CO_{bridge}$] and π acceptor [$RIn(I) < CO_{bridge}$] activities of the replacing ligand. Correspondingly, we have found for the analogous series with CF_2 and CH_2 bridges that the decrease of the Fe–Fe distance upon substitution is determined by the increasing π acceptor capability ($CO < CF_2 < CH_2$) [9].

In this paper, we present quantum chemical calculations, based on the density functional theory (DFT), for a number of $Fe_2(CO)_9$ derivatives with bridges potentially similar to CO. The bridging COs are replaced stepwise by any of the groups CH_2, CF_2, $SiMe_2$, $GeMe_2$, InMe and CS. Some of the examined compounds, with general formula $(CO)_3Fe(\mu\text{-}CO)_{3-n}(\mu\text{-}L)_nFe(CO)_3$ ($n =$ 0, 1, 2, 3) (see Scheme 1), are unknown experimentally, in particular those with one or more thiocarbonyl bridges. Also, not all of the experimentally known compounds feature exactly the inner dimetallic core with three bridging ligands (primary structure). Occasionally, in fact, the singly bridging or semi-bridging modes seem to be preferred. In the present investigation, however, we concentrate mainly on the triply bridging mode. In this manner, we can carry out direct and systematic comparisons of the bonding properties of the various bridges and of their expected effects on the primary structure of the binuclear system.

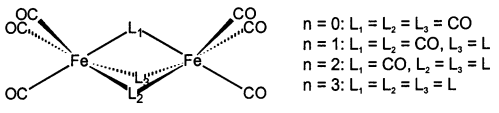

Scheme 1.

2. Computational details

DFT calculations applying the B3LYP [11] functionals were performed using the GAUSSIAN-98 program package [12]. For iron and indium, effective relativistic core potentials, replacing the ten and 46 inner-core electrons, respectively, were used together with the corresponding double-ζ 8s5p5d{341|311|41} and 3s3p{21|21}valence basis sets [13]. For the other atoms, the standard 6-31G* basis sets were used throughout [14].

Complete geometry optimizations were carried out under symmetry constraints which allow one to retain the presence of three bridges. Thus, with reference to the general structure of Scheme 1, we used D_{3h} symmetry for the case $n = 3$ and C_{2v} symmetry for the other cases with $n = 1$ and $n = 2$. For the InMe derivatives, the C_s and C_{3h} symmetries were exceptionally adopted for $n =$ 1 and $n = 3$, respectively, in order to account for the specific orientation of the methyl substituents.

Vibrational analyses were performed to characterize the stationary points of the optimized structures. For all of the systems with $n = 1$, an imaginary frequency of around 100 cm^{-1} is computed and the subsequent geometry optimizations at lower symmetry lead invariably to a singly bridged structure. This corresponds to the experimental result available for L = InMe [8c]. Contrasting results are instead observed for $L = CF_2$ and $L = CH_2$. In these cases, the X-ray analyses indicated a semi-bridged [9] and the symmetrically triple-bridged structure [2b], respectively. The computed $n = 2$ systems, with $L = CF_2$, CH_2, $SiMe_2$ and $GeMe_2$, as well as the $n = 3$ ones, with $L = CF_2$, CH_2 and CS, are genuine minima on the potential surface. Imaginary frequencies are also computed for the $n = 2$ system, with L = InMe, and for the $n = 3$ systems, with $L = SiMe_2$, $GeMe_2$ and InMe. These are evidently attributable to certain rotations of the methyl substituents and, by no means, they indicate the failure of a primary triple-bridged structure. A special case is the $n = 2$ system, with L = CS, which exhibits one imaginary frequency. The visual analysis of the latter suggests the movement of the bridging CO toward one iron center while the two CS groups vibrate toward the other metal.

The qualitative MO analyses were performed by adopting the EHMO method [15] with the usage of the weight-modified Wolfsberg–Helmholz formula [16]. After verifying that the numerical results are in line with the DFT response, the graphic utilities of the package CACAO [17] help to interpret the chemical bonding in terms of the classic perturbation theory concepts.

Table 1
Comparison of calculated and experimental (italics) structural parameters (in pm and °) for the complexes $Fe_2(CO)_{9-n}(\mu\text{-}L)_n$ with L = CO, CH_2, CF_2, $SiMe_2$, $GeMe_2$ and InMe

	CF_2 $n=2$	CH_2 $n=1$	CF_2 $n=1$	CO $n=3$	$SiMe_2$ $n=3$	$GeMe_2$ $n=3$	InMe $n=2$	InMe $n=3$
Fe–Fe	249.8	250.4	251.5	252.6	273.7	278.7	280.6	309.7
	246.9	*250.7*	*254.1*	*252.3*	*270.5*	*275.0*	*275.9*	*299.2*
Fe–L	201.0	202.2	201.1	200.8	237.2	242.0	255.2	255.3
	200.8	*202.2*	*197.4*	*201.6*	*232.2*	*239.8*	*258.1*	*258.2*
$Fe–CO_{br}$	200.8	200.7	200.7	200.8			200.9	
	198	*202.2*	*215.3*	*201.6*			*198.6*	
$Fe–C_{term}$	181.0	180.8	181.0	181.6	176.5	176.5	177.5	175.8
	182	*182.2*	*182*	*183.8*		*175.0*	*179.3*	*174.0*
$C–O_{term}$	114.5	114.7	114.6	114.7	115.7	115.7	115.4	116.4
	112.5		*113*	*115.6*		*117.0*	*114.3*	
Fe–L–Fe	76.8	76.5	77.4	79.0	70.5	70.3	66.7	74.7
	76.6	*76.8*	*80.1*	*77.6*		*70.0*	*64.6*	*70.8*
$Fe–C_{br}–Fe$	77.0	77.2	77.6	79.0			88.6	
	76.5	*76.8*	*72.3*	*77.6*			*88.0*	
Reference	[9]	[2b]	[9]	[18]	[4]	[5]	[8c]	[8d]

For $n=1$ and $n=2$, some values are given as averages.

3. Results and discussion

3.1. General structural trends and classification of the bridging ligands

Table 1 compares the computed and experimental structural parameters of the known di-iron carbonyls with three bridges of different nature. Although some individual deviations between calculated and experimental values amount to around 5%, the agreement is substantially good. Notice that the table is organized in the order of increasing Fe–Fe distance and that the latter is found to vary as much as 52.3 pm between the system with three InMe bridges and that with one CO and two CF_2 analogues. The corresponding computed difference of 59.9 pm indicates that the trend is satisfactorily reproduced. Only in the case of $L=CF_2$ and $n=1$, there is a certain amount of discrepancy, which becomes most evident for the $Fe–CO_{bridge}$ distance (the difference between experimental and computed values is ca. 15 pm). It must be recalled, however, that the available X-ray data [9] result from the superposition of two enantiomers with two semi-bridging CO ligands while the computed model has been forced to be triply bridged.

Complete sets of structural parameters which derive from our systematic calculations on the complexes with general formula $(CO)_3Fe(\mu\text{-}CO)_{3-n}(\mu\text{-}L)_nFe(CO)_3$ ($n=0, 1, 2, 3$) are conveniently presented in the Tables 2 and 3, for $L=CH_2$, CF_2 and CS (group I) and for $L=SiMe_2$, $GeMe_2$ and $InMe_2$ (group II), respectively. The subdivision is made on the basis that the Fe–Fe distance shortens stepwise for the group I bridges and elongates for the group II ones. Thus, it may stated that the intermetallic separation is the key indicator of the structural effects induced by the bridges of different nature.

Group I ligands always feature a bridging carbon atom (as the CO ligand itself) while, in the other case, a hetero-atom (Si, Ge, In) is involved. Fig. 1 summarizes graphically the trends affecting the Fe–Fe distance for an increasing number of bridge substitutions. Also, the overall graphic shows that for the same number of group I substituents, the iron–iron distance decreases in the order $CO > CF_2 \approx CS > CH_2$. Since the iron–bridge bond lengths are nearly invariant, the angles at the bridges decrease in the same order as the Fe–Fe distance itself. The bond lengths to the terminal carbonyl ligands as well as the terminal C–O bond lengths are not affected significantly from the substitution of the CO bridges with ligands of group I. These observations allow one to conclude that there is increasing attraction between the metal atoms for electronic reasons.

In contrast, the ligands of group II favour the increase of the Fe–Fe distance in the order $CO < SiMe_2 < GeMe_2 < InMe$. As a matter of fact, due to the increasing radius of the bridging hetero-atoms, the iron–bridge bond lengths increase in the same order. However, in the $n=3$ systems, the Fe–L–Fe bridging angles are always smaller than the corresponding $Fe–C_{br}–Fe$ angle in the parent complex. Thus, it may be inferred that the natural expansion of the system with the increasing size of the hetero-atom is contrasted by a direct attraction between the metals that has an electronic origin. An electronic cause must be also responsible for the slight decrease and increase of the terminal iron–carbonyl and C–O bond lengths, respectively. This aspect is observed for any series of compounds with a different bridge of group II.

Table 2
Calculated structural parameters (in pm and °) for $(CO)_3Fe(\mu\text{-}CO)_{3-n}(\mu\text{-}L)_nFe(CO)_3$ with L = CH_2, CF_2 and CS

		$n=0$	$n=1$	$n=2$	$n=3$
L = CH_2	Fe–Fe	252.6	250.4	246.3	241.0
	Fe–C_{br}(O)	200.8	200.7	201.0	
	Fe–C_{br}(H)		202.2	201.3	200.7
	C–O	117.0	116.8	116.4	
	C–H		109.2	109.2	109.2
	Fe–C_{term}	181.6	180.0/181.6	181.1/177.9	180.2
	C_{term}–O_{term}	114.7	114.8/114.7	114.8/114.9	114.9
	Fe–C_{br}(O)–Fe	79.0	77.2	75.6	
	Fe–C_{br}(H)–Fe		76.5	75.4	73.8
	Fe–Fe–C_{term}	120.4	119.8/121.0	119.9/120.7	120.3
	L–Fe–Fe–C(O)	120.0	117.5	124.3	120.0
L = CF_2	Fe–Fe		251.5	249.8	248.2
	Fe–C_{br}(F)		201.1	201.0	201.4
	Fe–C_{br}(O)		200.7	200.8	
	C–F		135.8	135.5	135.2
	C–O		116.7	116.6	
	Fe–C_{term}		180.9/182.7	182.3/179.8	181.4
	C_{term}–O_{term}		114.6/114.6	114.5/114.5	114.5
	Fe–C_{br}(F)–Fe		77.4	76.8	76.1
	Fe–C_{br}(O)–Fe		77.6	77.0	
	F–C–F		104.8	104.8	104.7
	Fe–Fe–C_{term}		121.4/119.6	120.0/123.3	121.5
	L–Fe–Fe–C(O)		117.7	123.3	120.0
L = CS	Fe–Fe		250.5	248.6	246.6
	Fe–C_{br}(S)		198.8	198.8	198.9
	Fe–C_{br}(O)		200.8	201.0	
	C_{br}–S		159.1	158.9	158.7
	C_{br}–O_{br}		116.9	116.8	
	Fe–C_{term}		181.5/182.3	182.3/181.4	182.2
	C_{term}–O_{term}		114.6/114.6	114.6/114.5	114.5
	Fe–C_{br}(S)–Fe		78.1	77.4	76.6
	Fe–C_{br}(O)–Fe		77.2	76.4	
	Fe–Fe–C_{term}		120.2/121.0	120.6/120.1	120.4
	L–Fe–Fe–C(O)		119.4	120.6	120.0

The first value of a pair in the systems with $n=1$ and $n=2$ refers to COs out of the Fe–bridge–Fe mirror plane, the second one to those in this plane.

We wish to anticipate at this point a general difference emerging from the detailed analysis of the electronic properties of group I and II ligands (vide infra). Although the ligands of both groups are better σ-donors and π-acceptors than CO (with the exception of InMe), it turns out that, for group I ligands, the π-acceptor capability has significantly more important geometric effects than the σ-donor one, whereas the opposite is true for the ligands of group II.

3.2. Orbital interactions at the bridging region

For the triply bridged complexes under investigation, it is relatively easy to separate into σ and π components the electronic interactions between the bridges and the fragment formed by the iron atoms and the terminal ligands. Thus, it is convenient to refer to the MO scheme of the parent $Fe_2(CO)_9$ system (Fig. 2) and to the selected MOs displayed in Fig. 3 (see also Ref. [19] for a more detailed description).

The symmetry combinations a_1' and e′ (D_{3h} symmetry) of the σ donor orbitals at the bridges match with the corresponding combinations of acceptor orbitals at the two metals. The bonding MOs a_1' and e′ are not only metal–bridge but also metal–metal bonding in character. Thus, the bridge-to-metal σ donation induces a certain amount of metal–metal attraction. The highest occupied MOs belong to the degenerate set 11e″ (at the higher left side of Fig. 3) which results from the interaction of carbonyl π* orbitals with antibonding combinations of hybridized d_π metal orbitals. Given the full population of the latter 11e″ set, each iron atom may be formally assigned the d^8 electron count. If, on one side, the 11e″ MOs give rise to two additional metal–bridge bonds, on the other side, they cause significant metal–metal repulsion on account of their metal–metal antibonding character [19,20]. The direct Fe–Fe bond,

Table 3
Calculated structural parameters (in pm and °) for $(CO)_3Fe(\mu\text{-}CO)_{3-n}(\mu\text{-}L)_nFe(CO)_3$ with L = $SiMe_2$, $GeMe_2$ and InMe

		$n=0$	$n=1$	$n=2$	$n=3$
L = $SiMe_2$	Fe–Fe	252.6	258.4	265.0	273.7
	Fe–Si		237.2	236.1	237.2
	Fe–C_{br}	200.8	200.2	200.1	
	C_{br}–O_{br}	117.0	117.1	117.1	
	Fe–C_{term}	181.6	179.2/180.4	178.4/177.3	176.5
	C_{term}–O_{term}	114.7	115.1/114.8	115.2/115.7	115.7
	Fe–Si–Fe		66.0	68.3	70.5
	Fe–C_{br}–Fe	79.0	80.4	82.9	
	Me–Si–Me		107.2	104.5	105.0
	Fe–Fe–C_{term}	120.4	121.6/116.4	119.4/119.4	119.8
	L–Fe–Fe–C(O)	120.0	115.0	120.8	120.0
L = $GeMe_2$	Fe–Fe		259.6	268.1	278.7
	Fe–Ge		241.9	241.2	242.0
	Fe–C_{br}		200.4	200.8	
	C_{br}–O_{br}		117.1	117.1	
	Fe–C_{term}		179.4/179.9	178.2/177.7	176.5
	C_{term}–O_{term}		115.1/114.8	115.2/115.6	115.7
	Fe–Ge–Fe		64.9	67.5	70.3
	Fe–C_{br}–Fe		80.7	83.7	
	Me–Ge–Me		107.8	104.8	105.0
	Fe–Fe–C_{term}		121.8/116.2	119.1/120.3	119.7
	L–Fe–Fe–C(O)		114.9	121.4	120.0
L = InMe	Fe–Fe		263.6	280.6	309.7
	Fe–In		256.3	255.2	255.3
	Fe–C_{br}		200.3	200.9	
	In–C		213.8	214.0	214.3
	C_{br}–O_{br}		117.3	117.5	
	Fe–C_{term}		179.5	177.1/177.9	175.8
	C_{term}–O_{term}		115,5	115.7/109.6	116.4
	Fe–In–Fe		61.9	66.7	74.7
	Fe–C_{br}–Fe		82.3	88.6	
	Fe–Fe–C_{term}			117.4/121.4	117.6
	L–Fe–Fe–C(O)		114.9	121.8	120.0

The first value of a pair in the systems with $n=1$ and $n=2$ refers to COs out of the Fe–bridge–Fe mirror plane, the second one to those in this plane. Averaged values for $n=1$ with L = InMe.

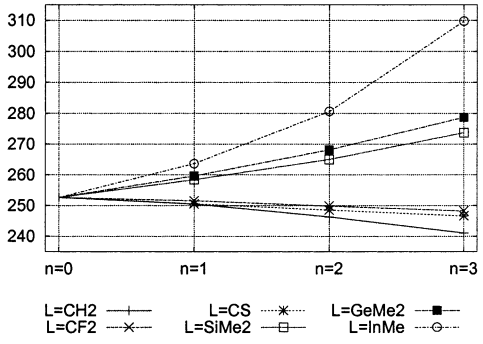

Fig. 1. Calculated Fe–Fe distances (pm) of the complexes $(CO)_3Fe(\mu\text{-}CO)_{3-n}(\mu\text{-}L)_nFe(CO)_3$.

which is assumed to exist on the basis of the 18-electron rule, can be recognized in connection with another type of metal–bridge backdonation. Consider that each metal, in its local octahedral environment, has three occupied 't_{2g}' orbitals which are formally nonbonding. The out-of-phase combination of two of them (essentially consisting of z^2 orbitals) matches the a_2'' combination of the carbonyl π* orbitals and some electron density is transferred into the latter. Due to this additional metal–bridge bonding, the overall z^2–z^2 interaction (orbital pair $14a_1'/10a_2''$ in Fig. 3) is no more four-electron repulsive and some effective metal–metal bonding character is acquired [19]. In any case, such a direct bonding interaction is weak and it is likely overwhelmed by the effective metal–metal repulsion induced by the formation of the metal-to-bridge acceptor bonds of e″ symmetry.

3.3. Donor/acceptor capabilities of the bridges

We turn now to the different electronic properties of the various bridging ligands. Concerning the donor/acceptor capabilities of these ligands, we first look at the orbital energies of their frontier orbitals which are depicted in Fig. 4.

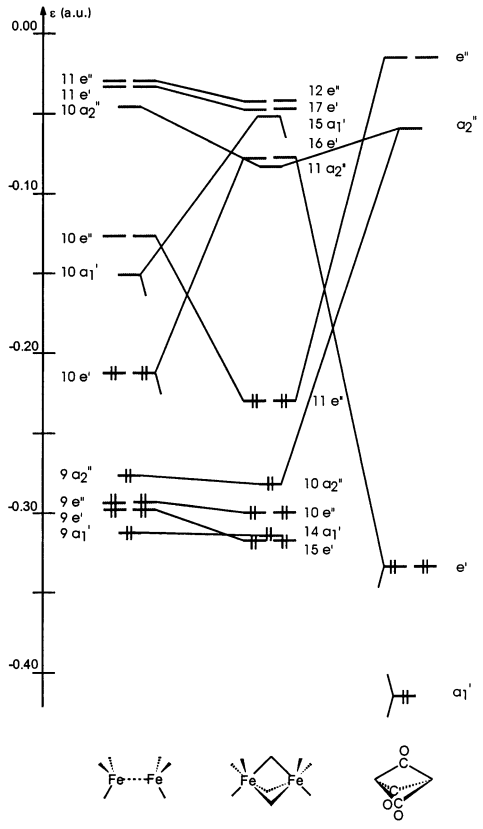

Fig. 2. Molecular orbital diagram for the parent $Fe_2(CO)_9$ system built up from a $(CO)_3Fe\cdots Fe(CO)_3$ fragment and the bridging $(CO)_3$ moiety.

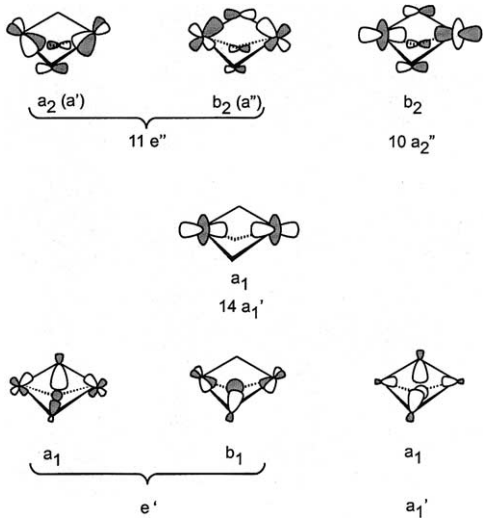

Fig. 3. Relevant molecular orbitals for a D_{3h} model of the type $(CO)_3Fe(\mu\text{-}L)_3Fe(CO)_3$. In most of the $n=1$ and $n=2$ derivatives of the type $(CO)_3Fe(\mu\text{-}CO)_{3-n}(\mu\text{-}L)_nFe(CO)_3$, the symmetry reduces to C_{2v} whose corresponding labels are indicated.

For each ligand, there is an orbital largely centered at the bridge atom that represents the σ lone pair. At higher energies, there is an acceptor orbital of π type, which is pure p_π at the bridging atom or is delocalized over the whole ligand molecule. The donor/acceptor

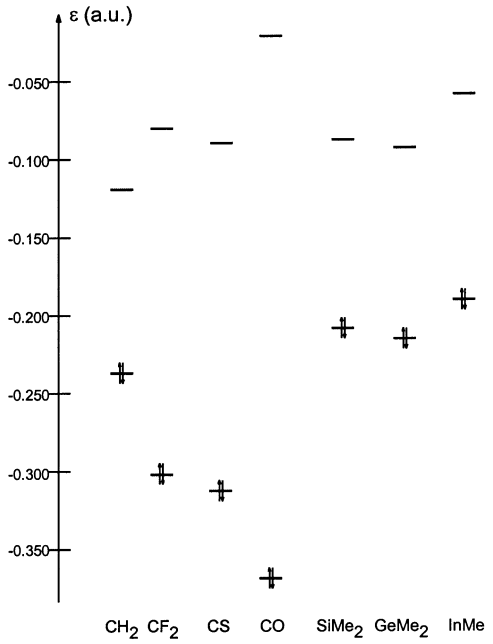

Fig. 4. Relative energy displacements of the donor/acceptor orbitals of the free ligands.

capabilities of the ligand are commonly related to the energies of these two levels. The higher is the filled σ orbital, the more donor it is. The lower lies the empty π-type orbital, the larger is its strength as an acceptor.

From its position in the scale of Fig. 4, we conclude that the carbonyl ligand is the weakest σ donor. By the same token, the ligands of group II are the best donors and we can order the bridge ligands in terms of the σ donor capability as follows: $CO < CS < CF_2 < CH_2 < GeMe_2 < SiMe_2 < InMe$. For the first four ligands, the order nicely matches the donor power list recently reported by Perrin et al. for a large series of different donors based on a computed evaluation of Tolman parameters [21]. Unfortunately, these authors did not take into account the ligands of our group II.

Considering the π acceptor orbitals, we find that CO is the weakest acceptor amongst the investigated ligands. The ligand CH_2 turns out to be the strongest one as its π acceptor function consists of a pure p_π carbon orbital, which is by symmetry strictly nonbonding. The acceptor orbitals of CF_2, CS as well as $SiMe_2$ and $GeMe_2$ are all in a somewhat higher energy region. For CF_2, CS (and CO), the orbital is destabilized compared to that of CH_2 because of its antibonding character, i. e. the negative overlap with the neighbor atom(s). InMe has a relatively high acceptor orbital, so it should be a weaker π acceptor than the other CO analogues. The following order of the π acceptor strength results: $CO < InMe < CS < CF_2 < SiMe_2 < GeMe_2 < CH_2$.

Among the CO analogues investigated, InMe is the strongest σ donor and the weakest π acceptor, whereas the other group II ligands, $SiMe_2$ and $GeMe_2$, are

somewhat weaker donors but better acceptors. CH_2 is a relatively good σ donor and the strongest π acceptor. The two remaining ligands, CF_2 and CS, are modest donors as well as acceptors. Looking at the free-ligand properties, i.e. the orbital energy of the π-acceptor orbital, InMe is expected to be a better π-acceptor than CO (Fig. 4). However, looking at the realized charge transfer in the complexes, InMe turns out to be the weakest π-acceptor (Table 5, Fig. 8).

To investigate in detail the intramolecular charge transfer, connected with the stepwise substitution of the bridging carbonyls in $Fe_2(CO)_9$, natural bond order (NBO) population analyses were performed [22]. In Tables 4 and 5, selected population values are reported.

The total populations at the bridges are separated into a σ and a π component (given in parentheses). The latter component results from the contributions of all of the p_π atomic orbitals (AOs) of the bridging ligand that are parallel to the Fe–Fe vector and that may be consequently involved in the backdonation (compare Fig. 3). The contributions of all of the remaining ligand AOs are collected in the σ part. We include in this part also the p_π orbitals that lie in the plane spanned by the bridging ligands and that may be only marginally involved in any interaction with metal orbitals.

From Table 4 and Fig. 5, one can infer that the population at the iron centers steadily decreases upon replacing bridging carbonyls with a ligand of group I. Because the population at the terminal ligands decreases as well, we recognize a modest global charge transfer toward the bridges (Fig. 6). This is opposite to what happens in the parent compound $Fe_2(CO)_9$ where a small charge (−0.045) transfers in the opposite direction. The separation of the charges into σ and π components shows that the bridging ligands of group I cause both a remarkable σ donation and π backdonation and that the latter effect prevails (compare Figs. 7 and 8 with Fig. 5).

Table 5 summarizes the NBO population analyses for the complexes with the bridging ligands of group II. Now, a steady increase of the population at the iron centers as well as at the terminal COs is featured (compare also with Fig. 5). A global charge is transferred toward the $Fe(CO)_3$ moieties (Fig. 6) and the metals reduce the 'donor pressure' from the bridges by forwarding some excess electron density to the terminal COs. By comparing Figs. 7 and 8, it is also evident that the σ donation prevails as there is only a modest π backdonation to the bridges. In particular, InMe appears to be a π acceptor even weaker than CO.

It is also possible to compare the donor/acceptor effects as they result from the whole systems with those predicted on the basis of the orbital energies of the free ligands (Fig. 4). For the σ donor strength, there is a complete agreement. The π acceptor strength of $SiMe_2$ and $GeMe_2$, however, is smaller than that of CF_2 and CS in contrast with what is predicted from the free-ligand properties alone. The π acceptor order is even

Table 4
NBO population analysis for $(CO)_3Fe(\mu\text{-}CO)_{3-n}(\mu\text{-}L)_nFe(CO)_3$ with L = CH_2, CF_2 and CS

		$n=0$	$n=1$	$n=2$	$n=3$
L = CH_2	Fe	16.577	16.527	16.476	16.419
	CH_2		8.176 (7.238/0.938)	8.166 (7.248/0.918)	8.130 (7.271/0.859)
	CO_{br}	13.985 (11.532/2.453)	13.972 (11.527/2.445)	13.938 (11.552/2.386)	
	Σbridges	41.955 (34.596/7.359)	36.120 (30.292/5.828)	30.270 (26.048/4.222)	24.390 (21.813/2.577)
	ΔΣbridges	−0.045 (−1.404/1.359)	0.120 (−1.708/1.828)	0.270 (−1.952/2.222)	0.390 (−2.187/2.577)
	CO_{term}	13.815	13.801/13.811	13.808/13.773	13.795
	ΔCO_{term}	−0.185	−0.199/−0.189	−0.192/−0.227	−0.205
L = CF_2	Fe		16.563	16.549	16.533
	CF_2		24.112 (19.360/4.752)	24.099 (19.369/4.730)	24.075 (19.384/4.691)
	CO_{br}		13.972 (11.518/2.454)	13.951 (11.529/2.422)	
	Σbridges		52.056 (42.396/9.566)	62.149 (50.267/11.882)	72.225 (58.152/14.073)
	ΔΣbridges		0.056 (−1.510/1.566)	0.149 (−1.733/1.882)	0.225 (−1.848/2.073)
	CO_{term}		13.796/13.816	13.803/13.772	13.785
	ΔCO_{term}		−0.204/−0.184	−0.197/−0.228	−0.215
L = CS	Fe		16.554	16.533	16.513
	CS		22.160 (17.456/4.704)	22.142 (17.460/4.682)	22.123 (17.457/4.666)
	CO_{br}		13.970 (11.510/2.460)	13.955 (11.509/2.446)	
	Σbridges		50.100 (40.476/9.624)	58.239 (46.429/11.810)	66.369 (52.370/13.998)
	ΔΣbridges		0.100 (−1.524/1.624)	0.239 (−1.571/1.810)	0.369 (−1.629/1.998)
	CO_{term}		13.794/13.807	13.787/13.772	13.768
	ΔCO_{term}		−0.206/−0.193	−0.213/−0.228	−0.232

The first value of a pair in the systems with $n=1$ and $n=2$ refers to COs out of the Fe–bridge–Fe mirror plane, the second one to those in this plane. σ and π components (see text) in parenthesis. The standard populations of the free fragments are: Fe, 16.000; CH_2, 8.000 (8.000/0.000); CF_2, 24.000 (20.000/4.000); CO, 14.000 (12.000/2.000); CS, 22.000 (18.000/4.000).

Table 5
NBO population analysis for $(CO)_3Fe(\mu\text{-}CO)_{3-n}(\mu\text{-}L)_nFe(CO)_3$ with L = $SiMe_2$, $GeMe_2$ and InMe

		$n=0$	$n=1$	$n=2$	$n=3$
L = $SiMe_2$	Fe	16.577	16.649	16.721	16.773
	$SiMe_2$		31.634 (29.040/2.594)	31.636 (29.068/2.568)	31.643 (29.093/2.550)
	CO_{br}	13.985 (11.532/2.453)	13.996 (11.531/2.465)	13.992 (11.540/2.452)	
	Σbridges	41.955 (34.596/7.359)	59.626 (52.102/7.524)	77.264 (69.676/7.588)	94.929 (87.279/7.650)
	ΔΣbridges	−0.045 (−1.404/1.359)	−0.374 (−1.898/1.524)	−0.736 (−2.324/1.588)	−1.071 (−2.721/1.650)
	CO_{term}	13.815	13.842/13.854	13.879/13.888	13.921
	ΔCO_{term}	−0.185	−0.158/−0.146	−0.121/−0.112	−0.079
L = $GeMe_2$	Fe		16.624	16.668	16.700
	$GeMe_2$		49.678 (43.073/6.605)	49.689 (43.104/6.585)	49.699 (43.134/6.565)
	CO_{br}		14.002 (11.536/2.466)	14.003 (11.550/2.453)	
	Σbridges		77.682 (66.145/11.537)	113.381 (97.758/15.623)	149.097 (129.401/19.695)
	ΔΣbridges		−0.318 (−1.855/1.537)	−0.619 (−2.242/1.623)	−0.903 (−2.598/1.695)
	CO_{term}		13.844/13.847	13.875/13.891	13.917
	ΔCO_{term}		−0.156/−0.153	−0.125/−0.109	−0.083
L = InMe	Fe		16.633	16.696	16.773
	InMe		11.222 (10.925/0.297)	11.258 (10.969/0.289)	11.321 (11.035/0.286)
	CO_{br}		14.043 (11.562/2.481)	14.088 (11.603/2.485)	
	Σbridges		39.308 (34.049/5.259)	36.604 (33.541/3.063)	33.963 (33.105/0.858)
	ΔΣbridges		−0.692 (−1.951/1.259)	−1.397 (−2.460/1.063)	−2.037 (−2.895/0.858)
	CO_{term}		13.880/13.916	14.041/13.981	14.081
	ΔCO_{term}		−0.120/−0.084	0.041/−0.019	0.081

The first value of a pair in the systems with $n=1$ and $n=2$ refers to COs out of the Fe–bridge–Fe mirror plane, the second one to those in this plane. σ and π components (see text) in parenthesis. The standard populations of the free fragments are: Fe, 16.000; $SiMe_2$, 32.000 (30.000/2.000); $GeMe_2$, 50.000 (44.000/6.000); InMe, 12.000 (12.000/0.000); CO, 14.000 (12.000/2.000).

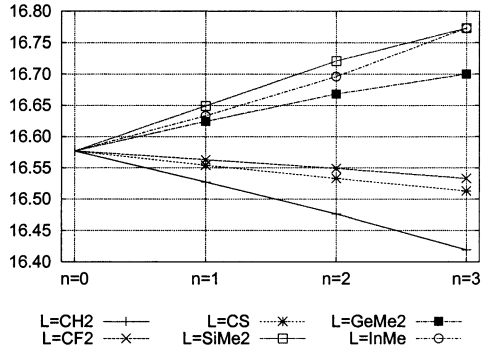

Fig. 5. NBO population at the iron centers in the systems $(CO)_3Fe(\mu\text{-}CO)_{3-n}(\mu\text{-}L)_nFe(CO)_3$.

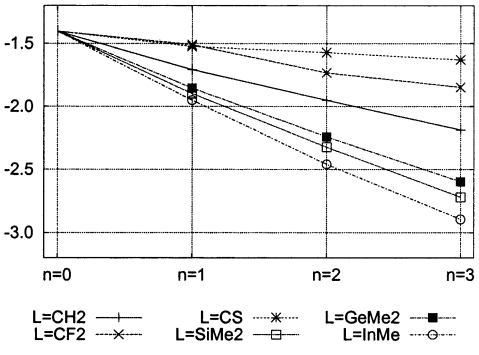

Fig. 7. NBO σ charge of the bridging moiety in the systems $(CO)_3Fe(\mu\text{-}CO)_{3-n}(\mu\text{-}L)_nFe(CO)_3$.

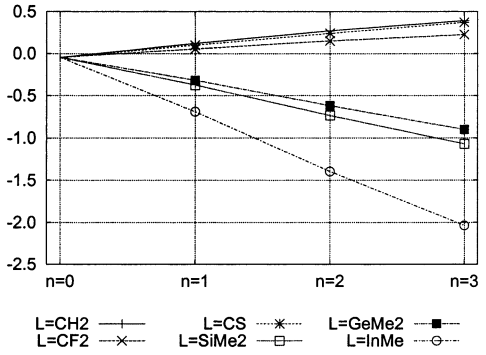

Fig. 6. NBO charge of the bridging moiety in the systems $(CO)_3Fe(\mu\text{-}CO)_{3-n}(\mu\text{-}L)_nFe(CO)_3$.

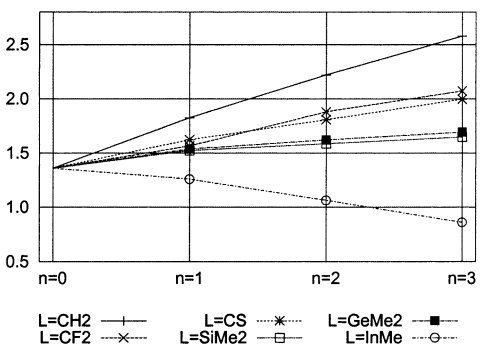

Fig. 8. NBO π charge of the bridging moiety in the systems $(CO)_3Fe(\mu\text{-}CO)_{3-n}(\mu\text{-}L)_nFe(CO)_3$.

reversed between CO and InMe. In conclusion, the extent of π backdonation involving the group II ligands cannot simply be described in terms of the corresponding orbital energies of the isolated ligands.

For a given type of bridge, the stepwise substitution within the parent compound $Fe_2(CO)_9$ affects the redistribution of the overall charge and of its components as illustrated by the single curves in Figs. 5–8. For complexes with group I ligands, the global charge transfer is directed toward the bridges, i.e. π backdonation exceeds σ donation. Nonetheless, it is evident from Table 4 that the global NBO population of each individual bridging ligand (including CO) decreases slightly along a series. The entering ligand has a stronger π acceptor capability than the leaving CO and prevents the other bridging groups from accepting the same amount of electron density as before. For complexes with group II ligands, the global charge transfer is directed from the bridges toward the iron tricarbonyl fragments, namely σ donation exceeds π backdonation. The NBO population of each individual bridging ligand increases due again to the competition between the bridges themselves. The entering ligand with a stronger σ donor capability than the leaving CO prevents the two other bridges from exerting the same donor power as before.

3.4. Relations between charge transfer and structural parameters

The computed results show clearly that the shortening of the Fe–Fe distance, upon progressive substitution for a bridging CO by a ligand of group I, is related to charge transferring toward the bridges. In contrast, the lengthening of the intermetallic distance, upon the progressive introduction of ligands of group II, is related to charge transferring away from the bridges.

The relation between charge transfer and Fe–Fe distance may be discussed in terms of the nature of some of the frontier molecular orbitals depicted in Fig. 3. Consider first the HOMOs e″ which are largely responsible for backdonation but also cause a repulsive interaction between the two metals. When a ligand of group I, with better π acceptor capability than CO, is progressively introduced ($n = 0 \rightarrow 3$), the electron density at the metals decreases. This is also reflected by the systematically reduced contribution of the iron orbitals to the HOMOs. Consequently, the metal–metal antibonding character of these MOs becomes less effective and the Fe–Fe distance is shortened.

It is also possible to provide a qualitative MO explanation for the relations between systems with a given number of hetero-bridges. For example, Fig. 9 shows the relative energies of the two degenerate e″ HOMOs for the various $n = 3$ systems. For the ligands of group I (with the exception of the CS case), the set is

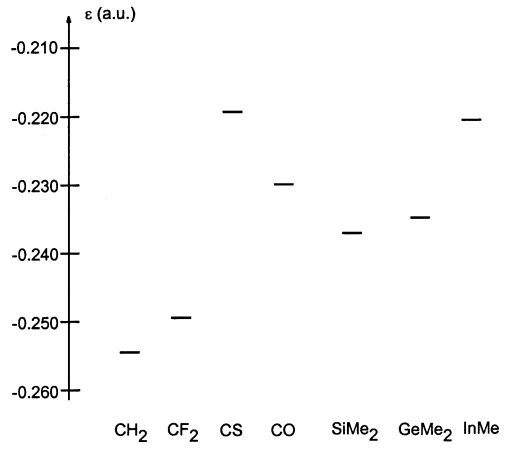

Fig. 9. Relative energy displacements of the HOMOs of the systems $(CO)_3Fe(\mu\text{-}L)_3Fe(CO)_3$.

lower than the corresponding one in $Fe_2(CO)_9$. In fact, the stronger π backdonation toward the non-CO bridges stabilizes significantly these MOs due to both strengthened Fe–bridge bonding and reduced Fe–Fe antibonding. Thus, a major cause for the decrease of the Fe–Fe distance is the different percentage composition of the HOMOs in presence of the various substituents.

Moreover, the third combination of the three π acceptor orbitals at the bridges (symmetric to threefold rotation) interacts with the out-of-phase combination of the occupied d_{z^2} metal orbitals to give rise to the lower lying MO a_2'' shown in Fig. 3. Such an interaction partially transforms the four-electron repulsion between z^2-based metal lone pairs into an attraction between the two iron centers. Thus, the substitution of the bridging COs by stronger π acceptor ligands reduces z^2–z^2 antibonding. For any given number of group I bridges, both the a_2'' and the e″ filled MOs (or their lower symmetry descendents) contribute to the decrease of the Fe–Fe separation.

If we now compare the complexes with a given number of group II bridges, the increase of the Fe–Fe distance in the series $CO < SiMe_2 < GeMe_2 < InMe$ is not uniquely related to one specific component of charge transfer (σ or π). The increasing atomic size of the bridging atoms certainly plays a role as the metal–bridge distances also increase consistently with the Fe–Fe distance. By overlooking, in a first approximation, any direct interaction between the iron centers, the progressively expanded Fe–bridge–Fe triangles should all be similar, i.e., the bridging bond angle should remain constant. However, the metals are not insensitive to each other. First of all, the longer Fe–bridge and Fe–Fe separations determine smaller overlaps between Fe atomic orbitals, hence, the intermetallic repulsion, stemming from the HOMOs, decreases. This is confirmed by bridge angles that are in any case smaller than in $Fe_2(CO)_9$ (see Table 3). Moreover, the minimum

angle is not found for the bridging atom with largest atomic size (consider that, in the indium derivative with $n = 3$, the Fe–L and the Fe–Fe distances are the longest). In fact, the calculations show that the Fe–L–Fe angles decrease in the order CO > InMe > $SiMe_2$ = $GeMe_2$. This is due to the balance of contrasting effects such as π backdonation and atomic size of the bridges. As shown in Fig. 8, the better π acceptors ($SiMe_2$ and $GeMe_2$) correspond to reduced iron contributions to the HOMOs with respect to the equivalent carbonyl case. The significantly diminished iron–iron repulsion with respect to the CO bridges is counterbalanced by the effect of larger atomic radii that impose longer Fe–Fe separations. The indium centered ligand, which has the largest atomic radius, appears to have reduced power as a π acceptor. This is highlighted by the higher energy of the HOMOs with respect to the equivalent group II systems and to the parent system itself (compare Fig. 9). For this reason, in the triply bridged InMe complex, the longest Fe–Fe separation is accompanied by relatively large Fe–In–Fe angles.

A certain amount of Coulomb repulsion between the metals can be expected due to the strong σ donation from the group II bridging ligands which might also affect the geometrical features. However, the change of the iron population upon substitution by different ligands does not parallel that of the bridge angles. In conclusion, the structural influence exerted by the group II bridging ligands is dominated by two major factors: their size and their π acceptor properties.

It is interesting to look at the terminal bond lengths of the complexes containing group II ligands. Both, the experimental and the calculated structures show an explicit decrease of the iron–carbon bond lengths and an increase of the C–O bond lengths compared to those of the parent $Fe_2(CO)_9$ system (see Table 3). This originates from the charge transfer effect caused by the strong σ donor power of the bridges. The electronic density that the metals receive from the bridges is partially transferred to the terminal carbonyls. This is, obviously, achieved through the mechanism of π back-donation as the Fe–CO_{term} bonds are strengthened and, at the same time, the C_{term}–O_{term} bonds are weakened. In contrast, group I ligands, which withdraw electron density from the metal centers, do not noticeably influence the bonding of the terminal carbonyl ligands.

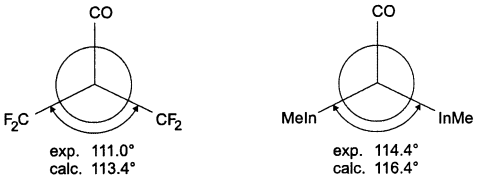

Scheme 2.

3.5. Break-up of the threefold symmetry in CF_2 and InMe derivatives

There is another structural peculiarity of the bridging moiety observed for the $n = 2$ systems with L = CF_2 and L = InMe. In both complexes, the respective torsion angles C(F_2)–Fe–Fe–C(F_2) and In–Fe–Fe–In are smaller than 120° (see Scheme 2), which is the ideal value consistent with the presence of a pseudo threefold axis in the system [8c,9]. At least for two coplanar CF_2 bridges, the feature is surprising as one would expect repulsion between neighboring fluorine atoms from the two different groups. Remarkably, the shortest contact between fluorine atoms is 279 pm, well below the sum of the van der Waals radii of 294 pm. On the other hand, CF_2 and InMe are representatives of the group I and group II ligands, respectively which, as shown, have opposite donor/acceptor properties.

The torsion angles resulting from the DFT optimizations are included in Scheme 2. The calculations reproduce the observed experimental trends and we can seek confidently their theoretical underpinnings.

We pursue the same strategy previously developed to highlight the attractive and repulsive interactions between the two iron centers in $Fe_2(CO)_9$ [19b]. The model is outlined as follows.

In the MO theory, bonding or antibonding interactions between two atoms are inferred from the positive or negative reduced overlap populations and, in particular, from the single contributions provided by selected molecular orbitals. For instance, the electrons occupying the 11e″ orbital pair (see Fig. 3) are, at one time, responsible for attractive iron–bridge and for repulsive iron–iron interactions. This picture, although merely qualitative, is extremely useful in chemistry. On the other hand, it is also possible to quantify more precisely the various components. By depopulating or populating a certain MO, one can artificially 'switch off' or 'switch on' the interactions generated by the orbitals under investigation. Subsequent geometry optimizations allow the system to relax under the modified conditions and, in general, increased or decreased bond distances are obtained. These changes can serve as a measure of the modified interatomic interactions.

Depopulation or population of the HOMO(s) and LUMO(s) is not simply feasible by adopting a cationic or an anionic derivative, respectively, of the species under investigation. A molecular charge of ±2 (or even higher) would cause additional intramolecular interactions that bias the results. Thus, in order to preserve the neutrality of the system, certain atoms of the molecule are substituted for by their neighbor elements in the periodic table having a smaller or a larger number of electrons. In this manner, the relaxation of the structure in going from real to model systems is dependent on the different number of electrons in selected parts of the

molecule. Indeed, the $Cr_2(CO)_9$ model system may be considered to have depopulated 11e″ levels, hence to 'switch off' the π acceptor interactions connected with these MOs. The optimization, in D_{3h} symmetry, leads to a structure, where only the σ donor interactions are effective in the bridging region. This structure shows very long metal–bridge distances and a somewhat smaller metal–metal distance compared to the actual $Fe_2(CO)_9$ complex [19b]. Alternatively, one can state that, by ''switching on'' the acceptor interactions, significant strengthening of the metal–bridge bonds occurs and that an effective repulsion between the two metals is triggered. The computed relaxation provides a quantitative answer to the points previously discussed in terms of orbital interactions and perturbation theory arguments [19a,20]. Importantly, the strategy confirms that a direct iron–iron attractive interaction is indeed detectable in $Fe_2(CO)_9$ [19b].

It must be emphasized that the model systems, which mimic the real ones with a different electron count, cannot be expected to be stable species as they are unreasonable from the chemical viewpoint. Thus, there is no guarantee that the optimization in a given symmetry will lead to a stationary point on the respective potential surface. But, if such a stationary point results, the specific relaxation of the structure caused by the missing or added electrons can provide useful pieces of information.

Table 6
Calculated structural parameters (in pm and °) for the model systems $(CO)_3M(\mu\text{-}CO)_{3-n}(\mu\text{-}CF_2)_nM(CO)_3$ (M = Fe, Mn and Cr)

		$n=0$	$n=1$	$n=2$	$n=3$ [a]
$(a_2)^2\ (b_2)^2$					
(M = Fe)	M–M	252.6	251.5	249.8	248.2
	M–C(F)		201.1	201.0	201.4
	M–C(O)	200.8	200.7	200.8	
	B–M–M–B	120.0	124.6	113.4	120.0
$(a_2)^0\ (b_2)^2$					
(M = Mn)	M–M	244.8	242.7	238.7	
	M–C(F) [b]	201.2	201.4	210.8	
	M–C(O)	210.3	209.5	200.5	
	B–M–M–B	103.5	107.9	98.8	
$(a_2)^2\ (b_2)^0$					
(M = Mn)	M–M	244.1	241.2	240.7	
	M–C(F) [b]	213.0	213.8	203.3	
	M–C(O)	203.7	202.8	216.5	
	B–M–M–B	127.9	128.9	143.5	
$(a_2)^0\ (b_2)^0$					
(M = Cr)	M–M	226.7	224.0	221.3	218.6
	M–C(F)		212.4	211.7	210.7
	M–C(O)	211.6	210.5	209.5	
	B–M–M–B	120.0	122.4	119.1	120
'Free bridge' [c]	B–X–B		122.4	122.2	

[a] No convergence for the Mn models.
[b] For $n=0$: M–C(O) with CO in the M–CO–M mirror plane.
[c] See text.

Table 7
Calculated structural parameters (in pm and °) for the model systems $(CO)_3M(\mu\text{-}CO)_{3-n}(\mu\text{-}InMe)_nM(CO)_3$ (M = Fe, Mn and Cr)

		$n=0$	$n=1$ [a,b]	$n=2$	$n=3$ [c]
$(a_2)^2\ (b_2)^2$					
(M = Fe)	M–M	252.6	263.6	280.6	309.7
	M–In		256.3	255.2	255.3
	M–C(O)	200.8	200.3	200.9	
	B–M–M–B	120.0	130.2	116.4	120.0
$(a_2)^0\ (b_2)^2$					
(M = Mn)	M–M	244.8	253.9	258.7	
	M–In [d]	201.2	259.0	262.6	
	M–C(O)	210.3	209.3	200.2	
	B–M–M–B	103.5	110.8	98.8	
$(a_2)^2\ (b_2)^0$					
(M = Mn)	M–M	244.1	249.7	263.7	
	M–In [d]	213.0	264.4	259.7	
	M–C(O)	203.7	202.6	211.7	
	B–M–M–B	127.9	136.1	129.2	
$(a_2)^0\ (b_2)^0$					
(M = Cr)	M–M	226.7		239.0	
	M–In			265.1	
	M–C(O)	211.6		210.5	
	B–M–M–B	120.0		116.6	
'Free bridge' [e]	B–X–B		138.2	98.2	

[a] a′ instead of a_2 and a″ instead of b_2 in the $n=1$ case (compare Fig. 3).
[b] No convergence for the Cr model.
[c] No convergence for the models with reduced electron number.
[d] For $n=0$: M–C(O) with CO in the M–CO–M mirror plane.
[e] See text.

We return to the various systems with L = CF_2 and L = InMe. For $n=2$ (C_{2v} symmetry, see the Introduction), the former D_{3h} 11e″ orbital set is split in two components of different energies (see Fig. 3). The corresponding labels a_2 and b_2 will also be used later for the C_s system with only one InMe bridge in place of the more appropriate a′ and a″ ones. The overall electronic population of the MOs is systematically decreased as metals Fe, Mn and Cr are introduced in the order. In particular, for the dimanganese system, a_2 and b_2 were alternatively populated.

Selected structural parameters resulting from the various optimizations are collected in Tables 6 and 7.

The complete 'switching off' of the π acceptor interactions by depopulating both the a_2 and b_2 frontier MOs (Cr in place of Fe) leads to a significant elongation of the metal–bridge bonds and shortening of the metal–metal distance, the latter as a result of the avoided metal–metal repulsion implicit in the 11e″ levels. When two Mn atoms are introduced (in place of Cr) only one of the two π acceptor interactions is turned on. If the level a_2 is populated, the interaction affects only the two bridges mirrored by the symmetry plane (see Fig. 3) and,

consequently, the corresponding metal–bridge bonds become shorter. The alternative population of the b_2 level mainly reduces the bond length to the unique bridge.

We focus now on the torsion angles bridge–M–M–bridge (denoted by B–M–M–B in Tables 6 and 7) by considering the $n=2$ systems, first. The values computed for the real systems $[(a_2)^2(b_2)^2$ configuration] are significantly smaller or larger for the models with an empty a_2 or b_2 MO, respectively. If both the MOs are empty, the torsion angles are again quite similar to those of the real systems. As mentioned, the population of only one MO (say a_2) 'switches on' only the π back-donation that involves the bridges other than the unique CO one. In turn, a repulsive interaction between the π systems of the two equivalent ligands is activated (see Fig. 3). This is substantiated by the increase of the torsion angle defined by the latter two ligands. The larger effect occurs in presence of two CF_2 bridges because CF_2 is a much better acceptor than InMe and the ligand contribution to the MO a_2 is larger. In contrast, the B–M–M–B torsion angle decreases when the MO b_2 is populated. In fact, there is repulsion between CO and each adjacent bridge, while the two equal groups are attracted to each other. In the dichromium system with two CF_2 bridges (empty a_2 and b_2 orbitals), the torsion angle turns out to be very close to 120°.

Finally, in the most realistic model $(CO)_3Fe(\mu\text{-}CO)(\mu\text{-}CF_2)_2Fe(CO)_3$, the observed $C(F_2)$–Fe–Fe–$C(F_2)$ torsion angle is a few degrees smaller than 120°. A direct comparison of the orbital coefficients shows that the contribution of the CF_2 groups is definitely larger in the a_2 than in the b_2 orbital (see Fig. 3). Thus, the π antibonding character between these two bridges exceeds the bonding one. At the same time, the composition of the b_2 MO indicates an antibonding interaction between the unique CO bridge and the CF_2 ones. The observed torsion angle results from a balancing of all the attractive and repulsive forces between the three bridges with a certain predominance of the antibonding CO–CF_2 interaction.

Also in the InMe case ($n=2$), the calculated torsion angle In–M–M–In is practically equal for the real system and its model with the a_2 and b_2 orbitals both empty. Consequently, the deviation from the ideal 120° value is not entirely attributable to the π trends imposed by the a_2 and b_2 MOs. There must be another reason, possibly connected with the bridge-to-metal σ donations or with another type of direct interaction between the bridging ligands.

To investigate such an origin, it is useful to perform partial optimizations of the various systems formed by the three bridging ligands, exclusively. To maintain the same inter-bridging interactions as in the actual metal complexes, the distances between the bridge donor

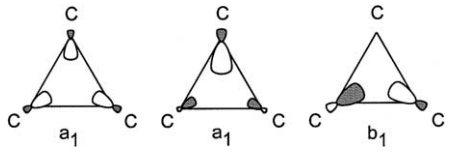

Scheme 3.

atoms and the midpoint X of the M–M binding line were kept fixed as well as the geometry of the individual bridges (the same as previously obtained from the optimization of the dichromium model). As a matter of fact, the partial optimizations concern only the angle B–X–B centered at the M–M midpoint and any pair of equal bridges in the various systems. Notice that this angle corresponds to the actual B–M–M–B torsion angle of the metal complexes. The ligand arrangement resulting from the optimizations reflects the relative amounts of direct bonding and antibonding interactions between the three bridging ligands themselves. Whereas these interactions, in the case of $L=CF_2$, seem to be rather symmetrically distributed (the B–X–B angle turns out to be 122.2°), a much more closed angle (98.2°) is found for L = InMe. The difference can be understood by looking at the combinations of the σ donor orbitals of the three ligands (see Schemes 3 and 4) that are also the three highest occupied MOs of the 'free bridge' systems.

In the CF_2 case ($n=2$), with three ligands of comparable σ donor capability (see Fig. 7), these MOs are very similar to those of any system with threefold symmetry ($n=0$, $n=3$) (Scheme 3). The mutual interactions between the three ligands are almost equal leading to a weak electron pair repulsion between all the donor pairs. In the InMe case, however, two strongly donating In orbitals combine with a much weaker donating CO orbital to form MOs of the composition schematically shown in Scheme 4. Now, the symmetric electron pair repulsion is distorted resulting in stronger repulsive and slightly attractive interactions. The In–In bonding components in the two a_1 orbitals overwhelm the antibonding component in b_1 giving rise to a significantly closed B–X–B angle (98.2°).

When the two InMe ligands bridge two $Cr(CO)_3$ fragments, a lot of electron density is donated to the electron-deficient metals and the direct interaction between the In σ hybrids is reduced. Accordingly, the angle considered increases to 116.6°. We conclude from this analysis that the torsion angle $<120°$, found in the

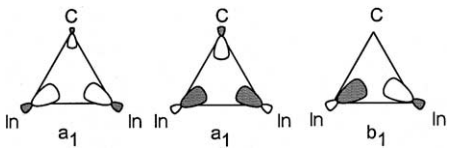

Scheme 4.

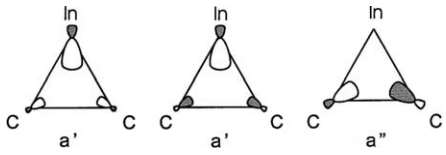

Scheme 5.

experimental and calculated complexes with two InMe bridges, is due to a direct In–In σ bonding interaction which persists in part when the ligands exert their bridging function.

Next, we consider the system with only one InMe bridge ($n = 1$). Recall that in this case the triply bridging network is idealized as the singly bridging coordination mode is observed experimentally. The depopulation of the a′ and a″ MOs leads, at first glance, to a relaxation similar to that found for the $n = 2$ system (compare the values in Table 7 with Fig. 3). For the 'free bridge' system $InMe(CO)_2$, however, the computed B–X–B angle is quite large (138.2°). This follows from the nature of the frontier MOs schematically shown in Scheme 5. Because of the strong donating σ hybrid at the unique In atom, the C(O)–C(O) antibonding component in a″ overwhelms the bonding ones which characterize the two a′ orbitals. Again, this effect is reduced (i.e., the angle decreases) upon the actual σ donation to the metal fragments. However, the repulsion between the two CO groups remains quite large and it can ultimately destabilize the symmetrically triple-bridged structure. This could be, at least, one of the reasons why the $n = 1$ InMe system is not triply but singly bridged.

The calculations do not show any remarkable differences concerning the σ donation in the $n = 2$ and $n = 1$ systems in the case of $L = CF_2$. Therefore, the torsion angle in the $n = 1$ system is primarily attributable to the π acceptor interactions. The calculated relaxation in going from the dichromium model system to the real one suggests that the antibonding interaction between the π systems of the two COs implicit in the a_2 orbital dominates (compare with Fig. 3). In analogy with the above arguments, such a repulsive interaction between the two CO groups, induced by the metal-to-bridge π backdonation, destabilizes somewhat the symmetrically triple-bridged structure. Thus, a semi-bridged functionality of the carbonyl ligands may be preferred.

4. Conclusions

In this article, we have reviewed the structural and electronic properties of binuclear iron systems with triads of bridging ligands of different nature. The analysis of the available structural data as well as of the computational results suggests that ligands, which are able to substitute systematically the carbonyls of the $Fe_2(CO)_9$ parent compound, can be catalogued in two different groups. In group I, the bridges still feature a pivotal carbon atom although linked to atoms other than oxygen. In group II, different hetero-atoms characterize the core of the bridging group. The geometry of the inner $Fe(\mu\text{-}L)_3Fe$ core changes significantly between the members of the different series. In particular, ligands of group I reduce the Fe–Fe distance compared to the parent $Fe_2(CO)_9$, whereas ligands of group II increase this distance. We have related these trends to the different σ and π bonding capabilities of the bridging ligands. The analysis confirms the very critical role of the electrons in the two HOMOs (e″ set for D_{3h} or its lower symmetry components). In fact, specific structural trends are clearly attributable to the latter frontier levels. Moreover, this study shows that the strength of the direct iron–iron attractive interaction assigned to the a_1'/a_2'' orbital pair is correspondingly modulated by the nature of the bridges.

Additionally, we have analyzed in detail the effects of the hetero-bridges on the primary threefold symmetry of the $Fe(\mu\text{-}L)_3Fe$ core. If, at first glance, reduced or enhanced separation between the bridges is alternatively attributable to bonding or antibonding interactions between their π systems, a more detailed study shows how also the different σ donor power of the bridges must be properly accounted for. The results have been achieved thanks to a peculiar technique based on the substitution of Fe with adjacent elements in the periodic table which allows us theoretically to 'switch on' or 'switch off' certain interactions within the complex systems.

Acknowledgements

We thank the Fonds der Chemischen Industrie and the Naturwissenschaftlich–Theoretisches Zentrum der Universität Leipzig for financial support. A.B. thanks the Deutsche Forschungsgemeinschaft for support through the Graduate Course 'Physical Chemistry of Interfaces'.

References

[1] C.E. Lukehart, Fundamental Transition Metal Organometallic Chemistry, Brooks/Cole Publishing Company, Monterey, 1985.
[2] (a) H. Werner, Angew. Chem. 102 (1990) 1109 (and references cited therein);
(b) B.B. Meyer, P.E. Riley, R.E. Davis, Inorg. Chem. 20 (1981) 3024.
[3] (a) G. Schmid, W. Petz, H. Nöth, Inorg. Chem. Acta 4 (1970) 423;
(b) H. Braunschweig, T. Wagner, Angew. Chem. 107 (1995) 904.
[4] R.S. Simons, C.A. Tessier, Acta Crystallogr. Sect. C 51 (1995) 1997.
[5] M. Elder, D. Hall, Inorg. Chem. 8 (1969) 1424.

[6] (a) C. Dohmeier, H. Krautscheid, H. Schnöckel, Angew. Chem. 106 (1994) 2570; Angew. Chem. Int. Ed. Engl. 33 (1994) 2482.;
(b) C. Üffing, A. Acker, R. Köppe, H. Schnöckel, Organometallics 17 (1998) 2373;
(c) J.T. Golden, T.H. Peterson, P.L. Holland, R.G. Bergman, R.A. Andersen, J. Am. Chem. Soc. 120 (1998) 223.
[7] (a) P. Jutzi, B. Neumann, G. Reumann, H.-G. Stammler, Organometallics 17 (1998) 1305;
(b) R. Fischer, M.M. Schulte, E. Herdtweck, M.R. Mattner, Inorg. Chem. 36 (1997) 2010;
(c) X. He, R.A. Bartlett, P.P. Power, Organometallics 13 (1994) 549;
(d) W. Uhl, M. Benter, M. Prött, J. Chem. Soc. Dalton Trans. (2000) 643.
[8] (a) W. Uhl, S.U. Keimling, W. Hiller, M. Neumayer, Chem. Ber. 128 (1995) 1137;
(b) W. Uhl, S.U. Keimling, W. Hiller, M. Neumayer, Chem. Ber. 129 (1996) 397;
(c) W. Uhl, S.U. Keimling, M. Pohlmann, S. Pohl, W. Saak, W. Hiller, M. Neumayer, Inorg. Chem. 36 (1997) 5478;
(d) W. Uhl, M. Pohlmann, Organometallics 16 (1997) 2478.
[9] W. Petz, F. Weller, A. Barthel, C. Mealli, J. Reinhold, Z. Anorg. Allg. Chem. 627 (2001) 1859.
[10] A. Barthel, C. Mealli, W. Uhl, J. Reinhold, Organometallics 20 (2001) 786.
[11] (a) A.D. Becke, J. Chem. Phys. 98 (1993) 5648;
(b) C. Lee, W. Yang, R.G. Parr, Phys. Rev. B 37 (1988) 785.
[12] M.J. Frisch, G.W. Trucks, H.B. Schlegel, G.E. Scuseria, M.A. Robb, J.R. Cheeseman, V.G. Zakrzewski, J.A. Montgomery, Jr., R.E. Stratmann, J.C. Burant, S. Dapprich, J.M. Millam, A.D. Daniels, K.N. Kudin, M.C. Strain, O. Farkas, J. Tomasi, V. Barone, M. Cossi, R. Cammi, B. Mennucci, C. Pomelli, C. Adamo, S. Clifford, J. Ochterski, G.A. Petersson, P.Y. Ayala, Q. Cui, K. Morokuma, D.K. Malick, A.D. Rabuck, K. Raghavachari, J.B. Foresman, J. Cioslowski, J.V. Ortiz, A.G. Baboul, B.B. Stefanov, G. Liu, A. Liashenko, P. Piskorz, I. Komaromi, R. Gomperts, R.L. Martin, D.J. Fox, T. Keith, M.A. Al-Laham, C.Y. Peng, A. Nanayakkara, M. Challacombe, P.M.W. Gill, B. Johnson, W. Chen, M.W. Wong, J.L. Andres, C. Gonzalez, M. Head-Gordon, E.S. Replogle, J.A. Pople, GAUSSIAN-98, Revision A.9, Gaussian Inc., Pittsburgh, PA, 1998.
[13] P.J. Hay, W.R.J. Wadt, J. Chem. Phys. 82 (1985) 299.
[14] W.J. Hehre, L. Radom, P.v.R. Schleyer, J. Pople, Ab-initio Molecular Orbital Theory, Wiley, New York, 1986.
[15] (a) R. Hoffmann, W.N. Lipscomb, J. Chem. Phys. 36 (1962) 2872;
(b) R. Hoffmann, W.N. Lipscomb, J. Chem. Phys. 37 (1962) 3489.
[16] J.H. Ammeter, H.-B. Bürgi, J.C. Thibeault, R. Hoffmann, J. Am. Chem. Soc. 100 (1978) 3686.
[17] (a) C. Mealli, D.M. Proserpio, J. Chem. Educ. 67 (1990) 399;
(b) C. Mealli, A. Ienco, D.M. Proserpio, Book of Abstracts of the XXXIII ICCC, Consiglio Nazionale delle Ricerche, Florence, 1998, p. 510.
[18] F.A. Cotton, J.M. Troup, J. Chem. Soc. Dalton Trans. (1974) 800.
[19] (a) C. Mealli, D.M. Proserpio, J. Organomet. Chem. 386 (1990) 203;
(b) J. Reinhold, E. Hunstock, C. Mealli, New J. Chem. 18 (1994) 465;
(c) E. Hunstock, C. Mealli, M.J. Calhorda, J. Reinhold, Inorg. Chem. 38 (1999) 5053.
[20] R.H. Summerville, R. Hoffmann, J. Am. Chem. Soc. 101 (1979) 3821.
[21] L. Perrin, E. Clot, O. Eisenstein, J. Loch, R.H. Crabtree, Inorg. Chem. 40 (2001) 5806.
[22] E.D. Glendening, A.E. Reed, J.E. Carpenter, F. Weinhold, NBO Version 3.1.